AdaptivePose: Human Parts as Adaptive Points

Yabo Xiao,[1] **Xiao Juan Wang,** [1,*] **Dongdong Yu,** [2] **Guoli Wang,** [3] **Qian Zhang,** [4] **Mingshu He** [1]

[1] Beijing University of Posts and Telecommunications
[2] ByteDance Inc.
[3] Tsinghua University
[4] Horizon Robotics

{xiaoyabo, wj2718, hemingshu}@bupt.edu.cn, yudongdong@bytedance.com, wangguoli1990@mail.tsinghua.edu.cn, qian01.zhang@horizon.ai

Abstract

Multi-person pose estimation methods generally follow top-down and bottom-up paradigms, both of which can be considered as two-stage approaches thus leading to the high computation cost and low efficiency. Towards a compact and efficient pipeline for multi-person pose estimation task, in this paper, we propose to represent the human parts as points and present a novel body representation, which leverages an adaptive point set including the human center and seven human-part related points to represent the human instance in a more fine-grained manner. The novel representation is more capable of capturing the various pose deformation and adaptively factorizes the long-range center-to-joint displacement thus delivers a single-stage differentiable network to more precisely regress multi-person pose, termed as AdaptivePose. For inference, our proposed network eliminates the grouping as well as refinements and only needs a single-step disentangling process to form multi-person pose. Without any bells and whistles, we achieve the best speed-accuracy trade-offs of 67.4% AP / 29.4 fps with DLA-34 and 71.3% AP / 9.1 fps with HRNet-W48 on COCO test-dev dataset.

Introduction

With the prevalence of deep learning technique, Pose estimation (Xiao et al. 2020; Newell, Yang, and Deng 2016) has drawn much attention in computer vision area. It's an essential step for many high-level vision tasks such as activity understanding (Shi et al. 2019; Li et al. 2019), pose tracking (Xiao, Wu, and Wei 2018) and so on. Most existing methods for multi-person pose estimation can be summarized in two ways including the top-down methods (Chen et al. 2018; Su et al. 2019; Sun et al. 2019; Fang et al. 2017) and the bottom-up methods (Cao et al. 2017; Kreiss, Bertoni, and Alahi 2019; Newell, Huang, and Deng 2017; Papandreou et al. 2018; Cheng et al. 2020). The top-down methods crop and resize the region of detected person firstly and then locate the single-person keypoints in each cropped region. These methods may have the following drawbacks: 1) The performance of joint detection is strongly tied to the quality of the human bounding boxes. 2) Detection-first pattern leads to high memory cost and low efficiency and is not feasible for applications. The bottom-up methods firstly locate the keypoints for the all persons simultaneously and then group them for each person. Although bottom-up methods generally run faster than top-down methods, the grouping process is still computationally complexity and redundant, and always involves many tricks to refine the final results.

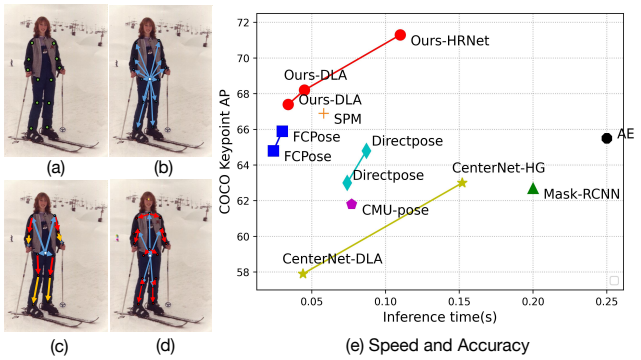

Figure 1: (a) Conventional body representation generally used in top-down methods such as Mask-RCNN (He et al. 2017) and Rmpe (Fang et al. 2017) as well as bottom-up methods such as CMU-pose (Cao et al. 2017) and AE (Newell, Huang, and Deng 2017). (b) Center-to-joint body representation proposed by CenterNet (Zhou, Wang, and Krähenbühl 2019). (c) Hierarchical body representation introduced by SPM (Nie et al. 2019). (d) An adaptive point set representation proposed by our method. (e) Inference time (s) versus precision (AP). Our method achieves the best speed-accuracy trade-offs compared with the representative bottom-up and single-stage methods.

Aforementioned two-stage methods generally use the conventional representation that models the human pose via absolute keypoint position as shown in Figure 1(a), which separates the associations between the human instance and keypoints thus requires an extra stage to model the relationship. Recent research works preliminarily explore the representation methods to model the relation between human instance and corresponding keypoints while suffer some obstacles thus leading to the limited performance. For exam-

*Corresponding author.

ple, as shown in Figure 1(b), CenterNet (Zhou, Wang, and Krähenbühl 2019) represents the human instance via center point and leverages center-to-joint offsets to form human pose but achieves the compromised performance since various pose deformation and the center has fixed receptive field thus hard to deal with long-range center-to-joint offsets. As shown in Figure 1(c), SPM (Nie et al. 2019) also represents the instance via root joint and further presents a fixed hierarchical tree-structure and divides the root joint and keypoints into four hierarchies based on articulated kinematics. It factorizes the long-range offsets into accumulative short ones while suffers the dilemma of accumulated error propagated along the skeleton.

To tackle with the aforementioned problems, In this work, we propose to represent the human parts as adaptive points and use an adaptive point set including the human center and seven human-part related points to fit diverse human instances. The human pose is formed in a body (center)-to-part (adaptive points)-to-joint manner, as shown in Figure 1(d). Compared with previous representations, the superiorities of our representation mainly involve in two aspects: 1) This fine-grained point set representation is more capable of capturing the various extent of deformation for human body compared with center representation. 2) It adaptively factorizes the long-range displacement into shorter ones while avoids the accumulated error propagated along the skeleton since the adaptive human-part related points are automatically learned by neural network.

Based on the adaptive point set representation, we propose an efficient end-to-end differentiable network, termed as AdaptivePose, which mainly consists of three novel components. First, we present a Part Perception Module to perceive the human parts by dynamically predicting seven adaptive human-part related points for each human instance. Second, in contrast to using the feature with fixed receptive field to predict the center of various bodies, Enhanced Center-aware Branch is introduced to conduct the receptive field adaptation and capture the various pose deformation by aggregating the features of adaptive human-part related points to perceive the center more precisely. Third, we propose a Two-hop Regression Branch where the adaptive human-part related points act as one-hop nodes to dynamically factorize long-range center-to-joint offsets. During inference, we only need a single-step decode process via combining the center positions and center-to-joint offsets to form human pose without any refinements and tricks.

The main contributions can be summarized as follows:

- We propose to represent human parts as points and further leverage an adaptive point set to represent the human instances. To our best knowledge, we are the first to present the fine-gained and adaptive body representation, which is more capable of capturing the various pose deformation and adaptively factorizes the long-range center-to-joint offsets.
- Based on the novel representation, we propose a compact single-stage differentiable network, termed as AdaptivePose. Specifically, we introduce a novel Part Perception Module to perceive the human parts by regressing seven human-part related points. By using human-part related points, we further propose an Enhanced Center-aware Branch to more precisely perceive the human center and a Two-hop Regression Branch to effectively factorize the long-range center-to-joint offsets.
- Our method significantly simplifies the pipeline of multi-person pose estimation and achieves the best speed-accuracy trade-offs of 67.4% AP / 29.4 fps , 68.2% AP / 22.2 fps with DLA-34, and 71.3% AP / 9.1 fps with HRNet-W48 on COCO test-dev set without any refinements and post-process.

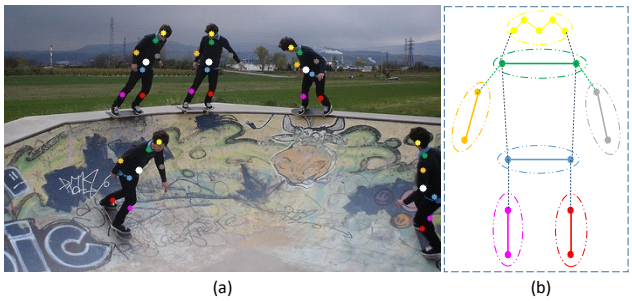

Figure 2: (a) The visualization of adaptive point set. White points indicate the human center and others refer to human-part related points visualized by colorful points corresponding the part with same color in Figure (b). (b) Divided human parts according to the degrees of freedom and extent of deformation. We leverage an adaptive point set conditioned on each human instance to represent the human in a fine-grained way.

Related Work

In this section, we review three parts related to our method including top-down methods, bottom-up methods and point-based representation methods.

Top-down Methods. Given an arbitrary RGB image, top-down methods firstly detect the location of human instance and then locate their keypoints individually. Concretely, the region of each human body would be cropped and resized to the unified size so that it has superior performance. Top-down methods mainly focus on the design of the network to extract better feature representation. HRNet (Sun et al. 2019) maintains high-resolution representations and repeatedly fuses multi-resolution representations through the whole process to generate reliable high-resolution representations. (Su et al. 2019) proposes a Channel Shuffle Module and Spatial, Channel-wise Attention Residual Bottleneck (SCARB) to drive the cross-channel information flow. However, due to inefficiency caused by the detection-first paradigm, top-down methods are often not feasible for the real-time systems with strict latency constraints.

Bottom-up Methods. In contrast to top-down methods, bottom-up methods localize keypoints of all human instances with various scales at first and then group them to the corresponding person. Bottom-up methods mainly concen-

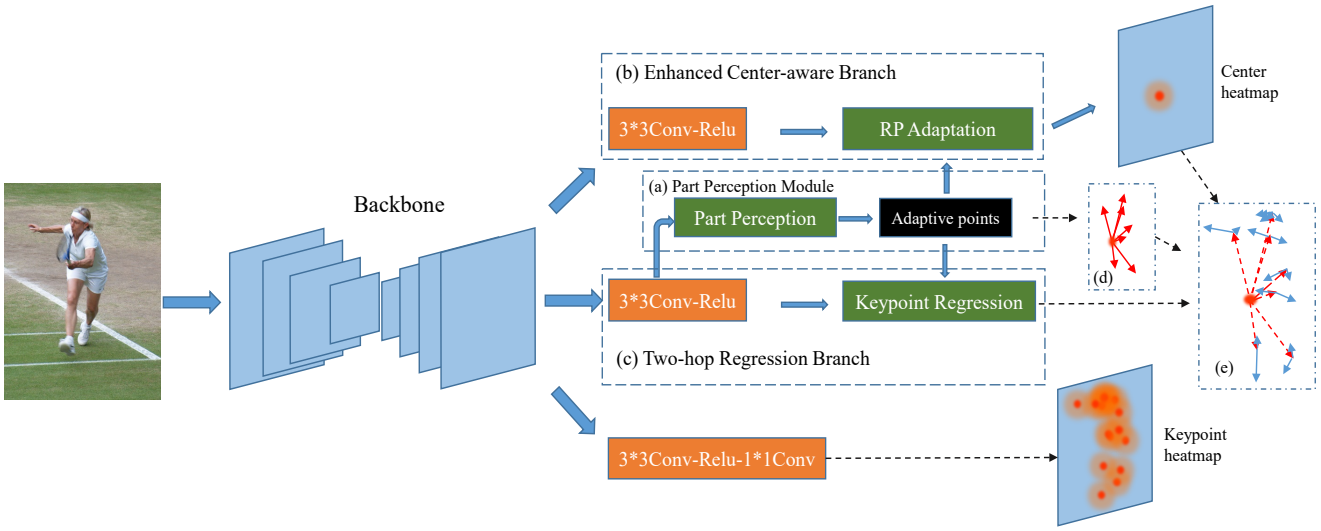

Figure 3: Overview of AdaptivePose. (a) The structure of Part Perception Module, Adaptive points indicate seven human-part related points. (b) The structure of Enhanced Center-aware Branch, RP Adaptation refers to receptive field adaptation. (c) The diagram of Two-hop Regression Branch. (d) The red arrows are one-hop offsets that dynamically locate the adaptive human-part related points. (e) The blue arrows indicate second-hop offsets for localizing the human joints.

trate on the effective grouping process. For example, CMU-pose (Cao et al. 2017) proposes a non parametric representation, named Part Affinity Fields (PAFs), which encodes the location and orientation of limbs, to group the keypoints to individuals in the image. AE (Newell, Huang, and Deng 2017) simultaneously outputs a keypoint heatmap and a tag heatmap for each body joint, and then assigns the keypoints with similar tags into individual. However, one case worth noting is that the grouping process serves as a post-process is still computationally complex and redundant.

Point-based Representation. The keypoint-based methods (Lee and Park 2020; Law and Deng 2018; Zhou, Wang, and Krähenbühl 2019; Nie et al. 2019; Tian, Shen, and Chen 2020) represent the instances by center or paired corners and have been applied in many tasks. They have drawn much attention as they are always simpler and more efficient than anchor-based representation (Cai and Vasconcelos 2018; Ren et al. 2015; Lin et al. 2017a,b; Huang et al. 2019; Liu et al. 2018). CenterNet proposes to use keypoint estimation to find center and then regresses the other object properties such as size to predict bounding box. SPM (Nie et al. 2019) represents the person via root joint and further presents a fixed hierarchical body representation to estimate human pose. Point-Set Anchors (Wei et al. 2020) propose to leverage a set of pre-defined points as pose anchor to provide more informative features for regression. DEKR (Geng et al. 2021) leverages the center to model the human instance and use a multi-branch structure that adopts adaptive convolutions to focus on each keypoint region for separate keypoint regression. In contrast to previous methods that use center or pre-defined pose anchor to model human instance, we propose to represent human instance via an adaptive point set including center and seven human-part related points as shown in Figure 2(a). The novel representation is able to capture the diverse deformation for human body and adaptively factorize long-range displacements.

Method

In this section, we firstly introduce our proposed body representation. Then, we elaborate on network architecture including each component. Finally, we report the training and inference details.

Body Representation

In contrast to previous body representation methods, we present an adaptive point set representation that uses the center point and seven human-part related points to represent the human instance in a fine-grained manner. The proposed representation introduces the adaptive human-part related points, which are used to finely-grained capture the structured human pose with various deformation and adaptively factorize the long-range center-to-joint offsets into shorter ones while avoids the accumulated error propagated along the fixed articulated skeleton.

In particular, we manually divide the human body into seven parts (i.e., face, shoulder, left arm, right arm, hip, left leg and right leg) according to the inherent structure of human body, as shown in Figure 2(b). Each divided human part is represented by an adaptive human-part related point, which is dynamically regressed from the human center. The process can be formulated as:

$$\mathbf{C}_{inst} \rightarrow \{\mathbf{P}_{face}, \mathbf{P}_{sho}, \mathbf{P}_{la}, \mathbf{P}_{ra}, \mathbf{P}_{hip}, \mathbf{P}_{ll}, \mathbf{P}_{rl}\}, \quad (1)$$

where $\mathbf{C}_{inst}$ refers to the instance center, others indicate seven adaptive human-part related points corresponding to

face, shoulder, left arm, right arm, hip, left leg and right leg. Human instance $inst$ is finely-grained represented by a point set $\{\mathbf{C}_{inst}, \mathbf{P}_{face}, \mathbf{P}_{sho}, \mathbf{P}_{la}, \mathbf{P}_{ra}, \mathbf{P}_{hip}, \mathbf{P}_{ll}, \mathbf{P}_{rl}\}$. For convenience, $\mathbf{P}_{part}$ is used to indicate the seven human-part related points $\mathbf{P}_{face}, \mathbf{P}_{sho}, \mathbf{P}_{la}, \mathbf{P}_{ra}, \mathbf{P}_{hip}, \mathbf{P}_{ll}, \mathbf{P}_{rl}$. Then we leverage human-part related points to locate the keypoints belong to corresponding parts as follows:

$$\mathbf{P}_{part} \rightarrow \mathbf{Joint}. \tag{2}$$

The novel representation starts from instance-wise (body center) to part-wise (adaptive human-part related points), then to joint-wise (body keypoints) to form human pose.

This fine-grained representation delivers a single-stage solution thus we present to build a single-stage differentiable regression network to estimate multi-person pose, where Part Perception Module is proposed to predict seven human-part related points. By using the adaptive human-part related points, Enhanced Center-aware Branch is introduced to perceive the center of human with various pose deformation and scales. In parallel, Two-hop Regression Branch is presented to regress keypoints via center-to-part-to-joint manner.

Single-Stage Network

Overall Architecture. As shown in Figure 3, given an input image, we first extract the general semantic feature via the backbone, followed by three well-designed components to predict specific information. We leverage Part Perception Module to regress seven adaptive human-part related points from the assumed center for each human instance. Then we conduct the receptive field adaptation in Enhanced Center-aware Branch by aggregating the features of the adaptive points to predict center heatmap. In addition, Two-hop Regression Branch adopts the adaptive human-part related points as one-hop nodes to indirectly regress the offsets from center to each keypoint.

Part Perception Module. Based on the novel representation, we artificially divide each human instance into seven fine-grained parts (i.e. face, shoulder, left arm, right arm, hip, left leg, right leg) according to the inherent structure of human body. Part Perception Module is proposed to perceive the human parts by predicting seven adaptive human-part related points. For each part, we automatically regress an adaptive point to represent it without any explicit supervision. As shown in Figure 4, the feature F_k is fed to the 3×3 convolutional layer to regress 14-channel x-y offsets from the center to seven adaptive human-part related points. These adaptive points act as intermediate nodes, which are used for subsequent predictions.

Enhanced Center-aware Branch. In previous works (Zhou, Wang, and Krähenbühl 2019; Nie et al. 2019), the center of human instances with various scales and pose are predicted via the feature with fixed receptive field for each position. We propose a novel Enhanced Center-aware Branch to aggregate the features of seven adaptive human-part related points for precise center estimation. It can be considered as receptive field adaptation process as well as capture the variation of pose deformation and scales.

As shown in Figure 4, We use the structure of 3×3 conv-relu to generate the branch-specific feature. In Enhanced

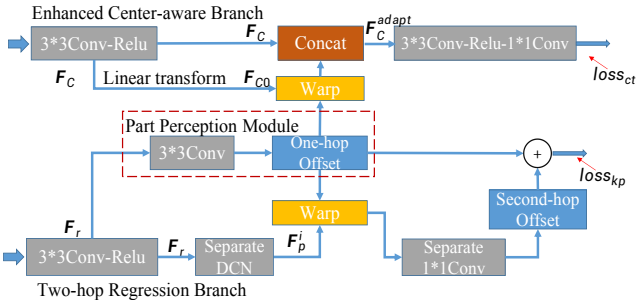

Figure 4: The detailed structure across the Part Perception Module, Enhanced Center-aware Branch and Two-hop Regression Branch. Linear transform indicates the feature compression along the channel dimension via 1*1 convolution. The red arrows is used to indicate where a loss is applied.

Center-aware Branch, $\mathbf{F}_c$ is branch-specific feature with the fixed receptive field for each position. We firstly conduct linear transform that compressing the feature $\mathbf{F}_c$ to obtain the squeezed feature $\mathbf{F}_{c0}$ and then extract the feature vectors of the adaptive points via bilinear interpolation on F_{c0}, which can be deemed as a warp operation mentioned in Figure 3. We named the extracted features as $\{\mathbf{F}_c^{face}, \mathbf{F}_c^{sho}, \mathbf{F}_c^{la}, \mathbf{F}_c^{ra}, \mathbf{F}_c^{hip}, \mathbf{F}_c^{ll}, \mathbf{F}_c^{rl}\}$ corresponding to seven manually divided human parts (i.e., face, shoulder, left arm, right arm, hip, left leg, right leg) and concatenate them with $\mathbf{F}_c$ to generate the feature $\mathbf{F}_c^{adapt}$. Since the predicted adaptive points located on the seven divided parts are relatively evenly distributed on the human body region, thus the process above can be regarded as the receptive field adaptation according to the human scale as well as finely-grained capture the various body deformation. Finally we use $\mathbf{F}_c^{adapt}$ with adaptive receptive field to predict the 1-channel probability map for the center localization.

We use a Gaussian distribution $\mathbf{G}_{xy} = \exp\left(-\frac{(x-C_x)^2+(y-C_y)^2}{2*\delta^2}\right)$ with mean (C_x, C_y) and adaptive variance δ to generate the ground-truth center heatmap. For the loss function of the Enhanced Center-aware Branch, we employ the pixel-wise focal loss in a penalty-reduced manner as follows:

$$loss_{ct} = \frac{1}{N}\sum_{n=1}^{N}\begin{cases} (1-\bar{P}_c)^{\alpha}\ \ln(\bar{P}_c) & if P_c = 1 \\ (1-P_c)^{\beta}\ \bar{P}_c^{\alpha}\ \ln(1-\bar{P}_c) & elif P_c \neq 1, \end{cases} \tag{3}$$

where N refers to the number of positive sample, $\bar{P}_c$ and P_c indicate the predicted confidence scores and corresponding ground truth. α and β are hyper-parameters and set to 2 and 4, following (Zhou, Wang, and Krähenbühl 2019).

Two-hop Regression Branch. We leverage a two-hop regression method to predict the displacements instead of directly regressing the center-to-joint offsets. In this manner, the adaptive human-part related points predicted by Part Perception Module act as one-hop nodes to adaptively factorize long-range center-to-joint offsets into center-to-part and part-to-joint offsets.

Similar to Enhanced Center-aware Branch, we firstly leverage the structure of 3×3 conv-relu to generate branch-specific feature, named $\mathbf{F}_r$ in Two-hop Regression Branch. Then we feed $\mathbf{F}_r$ into the separate deformable convolutions (Zhu et al. 2019; Dai et al. 2017) to generate separate features $\mathbf{F}_p^i$ for each human part. Then we extract the feature vectors at the adaptive points via a warp operation on corresponding feature $\mathbf{F}_p^i$. For convenience, we denote the extracted features as $\{\mathbf{F}_{face}, \mathbf{F}_{sho}, \mathbf{F}_{la}, \mathbf{F}_{ra}, \mathbf{F}_{hip}, \mathbf{F}_{ll}, \mathbf{F}_{rl}\}$ corresponding to seven divided parts (i.e., face, shoulder, left arm, right arm, hip, left leg and right leg). The extracted features are responsible for locating the keypoints belong to corresponding part by separate 1×1 convolutional layers. For example, $\mathbf{F}_{face}$ is used to localize the eyes, ears and nose, $\mathbf{F}_{la}$ is used to localize the left wrist and left elbow, $\mathbf{F}_{ll}$ is used to localize the left knee and left ankle.

Two-hop Regression Branch outputs a 34-channel tensor corresponding to x-y offsets $\bar{\mathbf{off}}$ from the center to 17 keypoints, which is regressed by a two-hop manner as follows:

$$\bar{\mathbf{off}} = \bar{\mathbf{off}}_1 + \bar{\mathbf{off}}_2, \tag{4}$$

where $\bar{\mathbf{off}}_1$ and $\bar{\mathbf{off}}_2$ respectively indicate the offset from center to adaptive human-part related point (one-hop offset mentioned in Figure 4) and the offset from human-part related point to specific keypoints (second-hop offset mentioned in Figure 4). The predicted offsets $\bar{\mathbf{off}}$ are supervised by L1 loss and the supervision only acts at positive keypoint locations, the other negative locations are ignored. The loss function is formulated as follows:

$$loss_{kp} = \frac{1}{K}\sum_{n=1}^{K}\left|\bar{\mathbf{off}}^n - \mathbf{off}_{gt}^n\right|, \tag{5}$$

where $\mathbf{off}_{gt}^n$ is the ground truth offset from center to each joint. K is the number of positive keypoint locations.

Training and Inference Details

During training, we employ an auxiliary training objective to learn keypoint heatmap representation, which enables the feature to maintain more human structural geometric information. In particular, we add a parallel branch to output a 17-channel heatmap corresponding to 17 keypoints and apply a Gaussian kernel with adaptive variance to generate ground truth keypoint heatmap. We denote this training objective as $loss_{hm}$, which is similar to Equation 3. The only difference is that N refers to the number of positive keypoints. The auxiliary branch is only used for training process and removed in inference process. Our total training target function for multi-task training process is formulated as:

$$loss_{total} = loss_{ct} + loss_{kp} + loss_{hm}. \tag{6}$$

During inference, Enhanced Center-aware Branch outputs the center heatmap that indicates whether the position is center or not. Two-hop Regression Branch outputs the offsets from the center to each joint. We firstly pick the human center by using 5×5 max-pooling kernel on the center heatmap to maintain 20 candidates, and then retrieve the corresponding offsets (δ_x^i, δ_y^i) to form human pose without any post-process and extra refinement. Specifically, we denote the predicted center as (C_x, C_y). The above decode process is formulated as follows:

$$(K_x^i, K_y^i) = (C_x, C_y) + (\delta_x^i, \delta_y^i), \tag{7}$$

where (K_x^i, K_y^i) is the coordinate of the i-th keypoint. In contrast to DEKR(Geng et al. 2021) that uses the average of the heat values at each regressed keypoints via bilinear interpolation, we only leverage the center heat-values as the pose score for fast inference.

Experiments and Analysis

In this section, we first briefly introduce the dataset, evaluation metric, data augmentation and implementation details. Next, we compare our proposed method with the previous state-of-the-art methods. Finally, we conduct comprehensive ablation study to reveal the effectiveness of each component.

Experimental Setup

Dataset. The COCO dataset (Lin et al. 2014) consists of over 200,000 images and 250,000 human instances labeled with 17 keypoints for pose estimation task. It is divided into train, mini-val, test-dev sets respectively. We train our model on COCO train2017 dataset. The comprehensive experimental results are reported on the COCO mini-val set with 5000 images and test-dev2017 set with 20K images.

Evaluation Metric. We leverage average precision and average recall based on Object Keypoint Similarity (OKS) to evaluate our keypoint detection performance.

Data Augmentation. During training, we use random flip, random rotation, random scaling and color jitter to augment training samples. The flip probability is 0.5, the rotation range is (-30, 30) and the scale range is (0.6, 1.3). Each input image is cropped according to the random center and random scale then resized to 512 / 640 pixels for DLA-34 (Yu et al. 2018) and 800 pixels for HRNet-W48 (Sun et al. 2019). The output size is 1/4 of the input resolution.

Implementation Details. We train our proposed model via Adam optimizer with a mini-batch size of 64 (8 per GPU) on a workstation with eight 12GB Titan Xp GPUs. We use initial learning rate of 2.5e-4. All codes are implemented with Pytorch. DLA-34 (19.7M) and HRNet-W48 (63.6M) are adopted to achieve the trade-off between the accuracy and efficiency. For inference, we keep the aspect ratio and resize the short side of the images to 512 / 640 / 800 pixels. The inference time is calculated on a 2080Ti GPU with mini-batch 1. We further use flip and multi-scale image pyramids to boost the performance. It is worth highlighting that the flip operation is only applied to the center heatmap predicted by Enhanced Center-aware Branch.

Main Results

Test-dev Results. As reported in Table 1, we compare our method with the previous state-of-the-art methods. In details, for bottom-up methods, our method achieves 67.4 AP, which outperforms the widely-used CMU-Pose (Cao et al. 2017), AE (Newell, Huang, and Deng 2017) as well as CenterNet-HG (Zhou, Wang, and Krähenbühl 2019) on

Methods	Params	AP	AP_{50}	AP_{75}	AP_M	AP_L	Time(s)
Bottom-up Heatmap-based Methods							
CMU-Pose*† (Cao et al. 2017)	-	61.8	84.9	67.5	57.1	68.2	0.077
AE*† (Newell, Huang, and Deng 2017)	227.8	65.5	86.8	72.3	60.6	72.6	0.25
CenterNet-DLA (Zhou, Wang, and Krähenbühl 2019)	-	57.9	84.7	63.1	52.5	67.4	0.044
CenterNet-HG (Zhou, Wang, and Krähenbühl 2019)	-	63.0	86.8	69.6	58.9	70.4	0.152
PersonLab (Papandreou et al. 2018)	68.7	66.5	88.0	72.6	62.4	72.3	-
PifPaf (Kreiss, Bertoni, and Alahi 2019)	-	66.7	-	-	62.4	72.9	-
HrHRNet-W48*† (Cheng et al. 2020)	63.8	70.5	89.3	77.2	66.6	75.8	0.182
FCPose (ResNet-101) (Mao et al. 2021)	-	65.6	87.9	72.6	62.1	72.3	0.093
SWAHR-W48* (Luo et al. 2021)	63.8	70.2	89.9	76.9	65.2	77.0	0.16
Single-stage Regression-based Methods							
SPM *† (Nie et al. 2019)	-	66.9	88.5	72.9	62.6	73.1	0.058
DirectPose † (Tian, Chen, and Shen 2019)	-	64.8	87.8	71.1	60.4	71.5	0.087
PointSetNet *† (Wei et al. 2020)	-	68.7	89.9	76.3	64.8	75.3	-
DEKR-W32*† (Geng et al. 2021)	29.6	69.8	89.0	76.6	65.2	76.5	0.192
DEKR-W48*† (Geng et al. 2021)	65.7	71.0	89.2	78.0	67.1	76.9	0.224
Ours (DLA-34)†	21.0	67.4	88.2	73.7	63.2	74.7	**0.034**
Ours (DLA-34+)†	21.0	68.2	89.0	75.1	64.6	75.0	0.045
Ours (HRNet-W48)†	64.7	**71.3**	**90.0**	**78.3**	**67.1**	**77.2**	0.110

Table 1: Comparisons with previous state-of-the-art methods on COCO test-dev set. $*$ indicates using extra test-time refinements. † refers to multi-scale testing. DLA-34+ indicates DLA-34 with 640 pixels input resolution. Note that the reported inference time of HigherHRNet (Cheng et al. 2020) and SWAHR (Luo et al. 2021) exclude the test refinement time.

Expt.	PPM	RFA	TR	AL	AP	AP_M	AP_L
1	-	-	-	-	56.0	47.3	68.4
2	√	√	-	-	57.3	48.7	69.1
3	√	-	√	-	60.0	51.7	71.0
4	√	√	√	-	61.6	85.2	72.8
5	√	√	√	√	**64.9**	**58.6**	**74.2**

Table 2: Ablation studies. PPM denotes Part Perception Module, RFA is receptive field adaptation conducted in Enhanced Center-aware Branch, TR indicates two-hop regression strategy in Two-hop Regression Branch, AL refers to employ an auxiliary loss $loss_{hm}$ to learn keypoint heatmap representation.

both performance and speed with a smaller model DLA-34. In contrast to HigherHRNet-W48 (Cheng et al. 2020) that uses higher resolution heatmap and test-time refinement to generate the final results, our approach with HRNet-W48 achieves 0.8 AP improvements without extra upsample and refinement operation.

For single-stage regression-based methods, AdaptivePose with HRNet-W48 surpasses SPM (Nie et al. 2019) (refined by the well-trained single-person pose estimation model) by 4.4% AP without any refinement and also outperforms DirectPose (Tian, Chen, and Shen 2019) with a large margin by 6.5% AP. In comparison to state-of-the-art DEKR (Geng et al. 2021), we achieve 0.3 AP gain without extra pose NMS and pose scoring network during inference. The comprehensive comparisons prove that our method achieves the better performance with the more efficient and compact pipeline.

Ablative Analysis

All ablation studies adopt DLA-34 as backbone and use the 1x training epoch (140 epochs) with single-scale testing on the COCO mini-val set.

Shared	AP	AP_{50}	AP_{75}	AP_M	AP_L	AR
-	64.2	86.0	70.3	57.9	73.6	69.9
√	**64.9**	**86.4**	**70.9**	**58.6**	**74.2**	**70.5**

Table 3: Shared refers to whether the adaptive points is shared between Enhanced Center-aware Branch and Two-hop Regression Branch.

Analysis of Part Perception Module. We conduct the controlled experiments to study the usage of Part Perception Module. As reported in Table 3, we respectively conduct the experiments that using shared adaptive points and unshared adaptive points (automatically locating seven positions via an additional 3×3 convolution) between Enhanced Center-aware Branch and Two-hop Regression Branch. Using the shared adaptive points obtains 0.7% AP improvements with less parameters and FLOPs compared with using unshared adaptive points (64.9% versus 64.2%). We consider that using the shared adaptive points is more interpretable since Part Perception Module is simultaneously supervised by $loss_{ct}$ and $loss_{kp}$ that mentioned in Equation 3 and 5. $loss_{ct}$ enables the adaptive points to more concentrate on the region with semantic information. $loss_{kp}$ drives the adaptive points to perceive the divided human parts so as to better conduct receptive field adaptation in Enhanced Center-aware Branch.

Analysis of Enhanced Center-aware Branch. We conduct the controlled experiments to explore the effect of receptive field adaptation process in Enhanced Center-aware Branch. Compared with using the feature with fixed receptive field to perceive the human center, receptive field adaptation process obtains 1.6% AP improvements in (Expt. 3 versus Expt. 4)

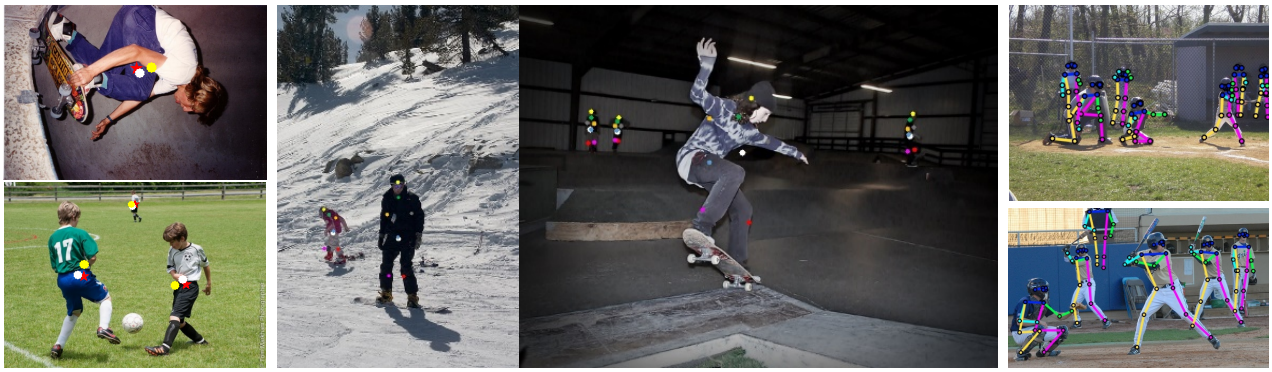

(a) (b) (c)

Figure 5: (a) Visualization of ground truth center (red star), the predicted center with receptive field adaptation (white point) and the predicted center without receptive field adaptation (yellow point). (b) Visualization of the predicted adaptive point set including the center and seven human-part related points for each human instance on COCO dataset. (b) Examples of predicted skeleton with various pose deformation on COCO dataset.

Methods	AP	AP_{50}	AP_{75}	AP_M	AP_L	AR
HKR	58.5	83.3	63.8	50.0	69.4	66.8
TR	**60.0**	**84.3**	**65.0**	**51.7**	**71.0**	**68.0**

Table 4: Comparisons between the hierarchical keypoint regression (notated as HKR) in SPM and our adaptive Two-hop Regression (notated as TR).

Methods	AP	AP_{50}	AP_{75}	AP_M	AP_L	AR
Ours-heat	64.6	**87.0**	70.3	58.0	74.1	69.7
Ours-reg	**64.9**	86.4	**70.9**	**58.6**	**74.2**	**70.5**

Table 5: Ablation study for exploring the effect of heatmap refinement for our two-hop regressed result.

of Table 2. The results prove that receptive field adaptation is capable of finely-grained capturing body deformation and dynamically adjusting the receptive field for the center of human instances with various scales, thus it is able to perceive the instance center more precisely. As shown in Figure 5(a), with receptive field adaptation, the predicted center is more closer to ground-truth center than without receptive field adaptation applied.

Analysis of Two-hop Regression Branch. We conduct the controlled experiments (Expt. 1 versus Expt. 3) in Table 2 to investigate the effect of two-hop regression. It brings to 4.0% AP improvements compared with directly regressing the displacements from center to each joints. Furthermore, based on Expt. 1, we implement the hierarchical body representation used in SPM to hierarchically regress the keypoint. As shown in Table 4. It drops 1.5 AP compared with our Two-hop Regression. The results prove our two-hop regression approach is capable of factorizing long-range center-to-joint offsets and avoiding the accumulated errors.

Analysis of auxiliary loss. (Expt. 4 versus Expt. 5) studies the effect of auxiliary loss, we achieve improvements of 3.3% AP by employing auxiliary loss to help training. It experimentally proves that the keypoint heatmap is able to retain more structural geometric information to improve regression performance.

Analysis of Heatmap Refinement for our regression result. For validating our regression performance, we further snap the closest confidence peaks on the keypoint heatmap to refine the regressed predictions. For convenience, the two-hop regressed result and the two-hop regressed result with heatmap refinement are denoted as Ours-reg and Ours-heat respectively. As shown in Table 5, Ours-reg obtain slightly better performance than Ours-heat (64.9% AP versus 64.6% AP), which proves the heatmap refinement is negligible for our two-hop regression method.

Qualitative Results. We visualize some qualitative results generated by our AdaptivePose. Figure 5(b) shows the predicted human center and seven adaptive human-part related points conditioned on each human instance with various scales and pose. The visualizations prove that the predicted adaptive human-part related points are able to finely-grained capture the human parts with various deformation and scales. In Figure 5(c), there are examples of the predicted skeleton on COCO mini-val set, which contain the diverse human bodies with various deformation.

Conclusion

In this paper, we propose to represent the human parts as points and introduce an adaptive body representation, which represents human body in a fine-grained fashion. Based on the proposed body representation, we construct a single-stage network, termed AdaptivePose, which including three effective components: Part Perception Module, Enhanced Center-aware Branch and Two-hop Regression Branch. During inference, we eliminate the grouping as well as refinements, and only need a single-step process to form human pose. We experimentally prove that AdaptivePose obtains the best speed-accuracy trade-off and outperforms previous state-of-the-art bottom-up and single-stage methods.

Acknowledgements

This work is supported by the National Natural Science Foundation of China (62071056) and the Doctorial Innovation Foundation of Beijing University of Posts and Telecommunications (CX2020111).

References

Cai, Z.; and Vasconcelos, N. 2018. Cascade r-cnn: Delving into high quality object detection. In *Proceedings of the IEEE conference on computer vision and pattern recognition*, 6154–6162.

Cao, Z.; Simon, T.; Wei, S.-E.; and Sheikh, Y. 2017. Realtime multi-person 2d pose estimation using part affinity fields. In *Proceedings of the IEEE conference on computer vision and pattern recognition*, 7291–7299.

Chen, Y.; Wang, Z.; Peng, Y.; Zhang, Z.; Yu, G.; and Sun, J. 2018. Cascaded pyramid network for multi-person pose estimation. In *Proceedings of the IEEE conference on computer vision and pattern recognition*, 7103–7112.

Cheng, B.; Xiao, B.; Wang, J.; Shi, H.; Huang, T. S.; and Zhang, L. 2020. HigherHRNet: Scale-Aware Representation Learning for Bottom-Up Human Pose Estimation. In *Proceedings of the IEEE/CVF Conference on Computer Vision and Pattern Recognition*, 5386–5395.

Dai, J.; Qi, H.; Xiong, Y.; Li, Y.; Zhang, G.; Hu, H.; and Wei, Y. 2017. Deformable Convolutional Networks. In *International Conference on Computer Vision*.

Fang, H.-S.; Xie, S.; Tai, Y.-W.; and Lu, C. 2017. Rmpe: Regional multi-person pose estimation. In *Proceedings of the IEEE International Conference on Computer Vision*, 2334–2343.

Geng, Z.; Sun, K.; Xiao, B.; Zhang, Z.; and Wang, J. 2021. Bottom-Up Human Pose Estimation Via Disentangled Keypoint Regression. In *Proceedings of the IEEE/CVF Conference on Computer Vision and Pattern Recognition*, 14676–14686.

He, K.; Gkioxari, G.; Dollár, P.; and Girshick, R. 2017. Mask r-cnn. In *Proceedings of the IEEE international conference on computer vision*, 2961–2969.

Huang, Z.; Huang, L.; Gong, Y.; Huang, C.; and Wang, X. 2019. Mask scoring r-cnn. In *Proceedings of the IEEE/CVF Conference on Computer Vision and Pattern Recognition*, 6409–6418.

Kreiss, S.; Bertoni, L.; and Alahi, A. 2019. Pifpaf: Composite fields for human pose estimation. In *Proceedings of the IEEE Conference on Computer Vision and Pattern Recognition*, 11977–11986.

Law, H.; and Deng, J. 2018. Cornernet: Detecting objects as paired keypoints. In *Proceedings of the European Conference on Computer Vision (ECCV)*, 734–750.

Lee, Y.; and Park, J. 2020. CenterMask: Real-time anchor-free instance segmentation. In *Proceedings of the IEEE/CVF Conference on Computer Vision and Pattern Recognition*, 13906–13915.

Li, M.; Chen, S.; Chen, X.; Zhang, Y.; Wang, Y.; and Tian, Q. 2019. Actional-structural graph convolutional networks for skeleton-based action recognition. In *Proceedings of the IEEE Conference on Computer Vision and Pattern Recognition*, 3595–3603.

Lin, T.-Y.; Dollar, P.; Girshick, R.; He, K.; Hariharan, B.; and Belongie, S. 2017a. Feature Pyramid Networks for Object Detection. In *Proceedings of the IEEE Conference on Computer Vision and Pattern Recognition (CVPR)*.

Lin, T.-Y.; Goyal, P.; Girshick, R.; He, K.; and Dollár, P. 2017b. Focal loss for dense object detection. In *Proceedings of the IEEE international conference on computer vision*, 2980–2988.

Lin, T.-Y.; Maire, M.; Belongie, S.; Hays, J.; Perona, P.; Ramanan, D.; Dollár, P.; and Zitnick, C. L. 2014. Microsoft coco: Common objects in context. In *European conference on computer vision*, 740–755. Springer.

Liu, S.; Qi, L.; Qin, H.; Shi, J.; and Jia, J. 2018. Path aggregation network for instance segmentation. In *Proceedings of the IEEE conference on computer vision and pattern recognition*, 8759–8768.

Luo, Z.; Wang, Z.; Huang, Y.; Wang, L.; Tan, T.; and Zhou, E. 2021. Rethinking the Heatmap Regression for Bottom-up Human Pose Estimation. In *Proceedings of the IEEE/CVF Conference on Computer Vision and Pattern Recognition*, 13264–13273.

Mao, W.; Tian, Z.; Wang, X.; and Shen, C. 2021. FCPose: Fully Convolutional Multi-Person Pose Estimation with Dynamic Instance-Aware Convolutions. In *Proceedings of the IEEE/CVF Conference on Computer Vision and Pattern Recognition*, 9034–9043.

Newell, A.; Huang, Z.; and Deng, J. 2017. Associative embedding: End-to-end learning for joint detection and grouping. In *Advances in neural information processing systems*, 2277–2287.

Newell, A.; Yang, K.; and Deng, J. 2016. Stacked Hourglass Networks for Human Pose Estimation. In *European Conference on Computer Vision*.

Nie, X.; Feng, J.; Zhang, J.; and Yan, S. 2019. Single-stage multi-person pose machines. In *Proceedings of the IEEE International Conference on Computer Vision*, 6951–6960.

Papandreou, G.; Zhu, T.; Chen, L.-C.; Gidaris, S.; Tompson, J.; and Murphy, K. 2018. Personlab: Person pose estimation and instance segmentation with a bottom-up, part-based, geometric embedding model. In *Proceedings of the European Conference on Computer Vision (ECCV)*, 269–286.

Ren, S.; He, K.; Girshick, R.; and Sun, J. 2015. Faster r-cnn: Towards real-time object detection with region proposal networks. In *Advances in neural information processing systems*, 91–99.

Shi, L.; Zhang, Y.; Cheng, J.; and Lu, H. 2019. Two-stream adaptive graph convolutional networks for skeleton-based action recognition. In *Proceedings of the IEEE Conference on Computer Vision and Pattern Recognition*, 12026–12035.

Su, K.; Yu, D.; Xu, Z.; Geng, X.; and Wang, C. 2019. Multi-person pose estimation with enhanced channel-wise and spatial information. In *Proceedings of the IEEE Conference on Computer Vision and Pattern Recognition*, 5674–5682.

Sun, K.; Xiao, B.; Liu, D.; and Wang, J. 2019. Deep high-resolution representation learning for human pose estimation. In *Proceedings of the IEEE conference on computer vision and pattern recognition*, 5693–5703.

Tian, Z.; Chen, H.; and Shen, C. 2019. DirectPose: Direct End-to-End Multi-Person Pose Estimation. *arXiv preprint arXiv:1911.07451*.

Tian, Z.; Shen, C.; and Chen, H. 2020. Conditional Convolutions for Instance Segmentation. *arXiv preprint arXiv:2003.05664*.

Wei, F.; Sun, X.; Li, H.; Wang, J.; and Lin, S. 2020. Point-set anchors for object detection, instance segmentation and pose estimation. In *European Conference on Computer Vision*, 527–544. Springer.

Xiao, B.; Wu, H.; and Wei, Y. 2018. Simple baselines for human pose estimation and tracking. In *Proceedings of the European conference on computer vision (ECCV)*, 466–481.

Xiao, Y.; Yu, D.; Wang, X.; Lv, T.; Fan, Y.; and Wu, L. 2020. SPCNet:Spatial Preserve and Content-aware Network for Human Pose Estimation. In *European Conference on Artificial Intelligence*.

Yu, F.; Wang, D.; Shelhamer, E.; and Darrell, T. 2018. Deep layer aggregation. In *Proceedings of the IEEE conference on computer vision and pattern recognition*, 2403–2412.

Zhou, X.; Wang, D.; and Krähenbühl, P. 2019. Objects as points. *arXiv preprint arXiv:1904.07850*.

Zhu, X.; Hu, H.; Lin, S.; and Dai, J. 2019. Deformable ConvNets V2: More Deformable, Better Results. In *Computer Vision and Pattern Recognition*.